https://doi.org/10.5194/bg-2019-477
Preprint. Discussion started: 12 February 2020

Biogeosciences Discussions
Open Access
EGU

Vegetation Influence and Environmental Controls on Greenhouse Gas Fluxes from a Drained Thermokarst Lake in the Western Canadian Arctic

June Skeeter[1], Andreas Christen[2], Andrée-Anne Laforce[3], Elyn Humphreys[3], Greg Henry[1]

[1]Department of Geography, The University of British Columbia, Vancouver, V6T1Z2, Canada
[2]Environmental Meteorology, Faculty of Environment and Natural Resources, Albert-Ludwigs Universität Freiburg, Freiburg, Germany
[3]Department of Geography and Environmental Studies, Carleton University, Ottawa, K1S5B6, Canada

Correspondence to: June B. Skeeter (skeeter1@mail.ubc.ca)

Abstract. Thermokarst features are widespread in ice-rich regions of the circumpolar Arctic. The rate of thermokarst lake formation and drainage is anticipated to accelerate as the climate warms. However, it is uncertain how these dynamic features impact the terrestrial Arctic carbon cycle. Methane (CH_4) and carbon dioxide (CO_2) fluxes were measured during peak growing season using eddy covariance and chambers at Illisarvik, a 0.16 km^2 thermokarst lake basin that was experimentally drained in 1978 on Richards Island, Northwest Territories, Canada. Vegetation in the basin differs markedly from the surrounding dwarf-shrub tundra and included patches of tall shrubs, grasses and sedges with some bare ground and a small pond in the centre. During the study period, temperature and wind conditions were highly variable and soil water content decreased steadily. Basin scaled net ecosystem exchange (NEE) measured by eddy covariance was -1.5 [$CI_{95\%}$ ± 0.2] g C-CO_2 m^{-2} d^{-1}; NEE followed a marked diurnal pattern with no trend during the study period. NEE was primary controlled by photosynthetic photon flux density and influenced by vapor pressure deficit, volumetric water content and the presence of shrubs. By contrast, net methane exchange (NME) was low (8.7 [$CI_{95\%}$ ± 0.4] mg CH_4 m^{-2} $d^{-1}$and had little impact on the carbon balance of the basin during the study period. NME displayed high spatial variability, sedge areas in the basin were the strongest source of CH_4 while upland areas outside the basin were a net sink. Soil moisture and temperature were the main environmental factors influencing NME, having a positive and negative effect respectively.

Keywords: Climate Change, Arctic, Permafrost, Thermokarst, Carbon, Methane

1 Introduction

Thermokarst lakes are a widespread feature in poorly drained, sedimentary permafrost lowlands with excess ground ice volume (French, 2013). These lakes drain, sometimes catastrophically, via bank overflow, ice wedge erosion, coastal erosion, and stream migration (Billings and Petersons, 1980; Mackay, 1999). Thermokarst lakes and drained thermokarst lake basins (DTLB) are prominent landscape features of the western Canadian Arctic (Mackay, 1999; Marsh et al, 2009; Lantz & Turner, 2015). Lake formation and drainage is a natural part of the thaw lake cycle, but it

https://doi.org/10.5194/bg-2019-477
Preprint. Discussion started: 12 February 2020

is anticipated that climate change will accelerate this cycle resulting in more lake formation and drainage (Jones et al., 2018).

Thermokarst lakes are well recognized sources of methane (CH_4) which is 28 times as potent as carbon dioxide (CO_2) on a 100-year time scale (Walter et al., 2007). Thermokarst lake formation and expansion is expected to exert a positive feedback on climate change and accelerate Arctic warming in the near term, but one modelling study suggests that drainage may limit expansion and result in decreased lake area by the end of the century (van Huissteden et al., 2011). Post drainage, DTLB undergo rapid ecological succession. In colder tundra environments, meadows or polygonal landscapes dominated by sedges, grasses and rushes will form (Lara et al., 2015). In slightly warmer, boreal or transitional regions, DTLB often become dominated by willows and other shrubs (Lantz and Turner, 2015). Carbon exchange in DTLB of various ages has been examined by a few studies, all of which focused on the Barrow Peninsula in Northern Alaska. In general, DTLB are net sinks for CO_2 with greatest uptake in younger basins and decreasing net uptake of CO_2 as the basin ages (Zona et al., 2010; Zulueta et al., 2011; Lara et al., 2015). DTLB source/sink strength of CH_4 was found to be highly variable depending on vegetation and ground conditions (Lara et al., 2015). Net methane exchange (NME) is highest in wet or flooded meadows and remnant ponds while upland tundra surrounding DTLB can be a methane sink (Zona et al., 2009; Zona et al., 2012; Lara et al., 2015; Sturtevant and Oechel, 2013).

In this study, fluxes of CO_2 and CH_4 were measured at Illisarvik, an experimentally drained thermokarst lake bed on Richard's Island in the western Canadian Arctic, Northwest Territories, Canada. Fluxes of CO_2 and CH_4 were measured during the peak growing season using a combination of closed chamber and eddy covariance (EC) measurements. Net ecosystem exchange (NEE) of CO_2 was calculated from fluxes and storage change and NEE was separated into ecosystem respiration (ER) and gross primary productivity (GPP), $NEE = ER + GPP$. Here we report on: 1) the spatial and temporal variability of the NEE and NME, 2) the vegetation and environmental factors NEE and NME, 3) how the carbon balance at Illisarvik compares to other DTLB, and 4) potential future trajectories as Illisarvik continues to evolve.

2 Methods

2.1 Study Site and Data Collection

The study took place at Illisarvik, a DTLB on Richards Island (69˚28'47.5" N, 134˚35'18.7" W), that was drained experimentally in 1978 (Mackay, 1981). Illisarvik has since served as the focus of studies on permafrost growth, active layer development and vegetation succession (Ovenden, 1986; Mackay and Burn, 2002; O'Neil et al., 2012; Wilson et al., 2019). At the nearby Tuktoyaktuk climate station mean annual air temperature (T_a) is -10°C, July is the warmest month with a mean of 11°C and January is the coldest at -27°C. Mean annual precipitation is 160.7 mm yr^{-1}, the majority falling as rain in the summer and autumn. Snow cover typically lasts from September or October to late May (Environment Canada. 2016). Tuktoyaktuk is 60 km east of Illisarvik and in similar proximity to the coast so the climatology is expected to be similar at Illisarvik.

https://doi.org/10.5194/bg-2019-477
Preprint. Discussion started: 12 February 2020

In the 39 years since drainage, Illisarvik has undergone rapid vegetation succession. After drainage, there were two remnant ponds. In the first five years after drainage, vegetation colonized the basin margins and wetter areas (Ovenden, 1986). By 1999, low vegetation had proliferated across most of the basin and taller willows had become established along the basin margins (Mackay and Burn; 2002). By 2010, some of the willows had grown to be 3 m in height (O'Neil and Burn; 2012). Current vegetation at Illisarvik is diverse relative to the dwarf-shrub tundra of the surrounding uplands; the basin hosts a mix of woody shrubs (*Salix* spp., *Betula* spp., & *Alnus* spp), wetland vegetation (*Carex* spp.,*Arctophila fulva*, etc.), and various grasses (Pocacea spp.). The basin is partly ringed by a terrace of peat that formed after a partial drainage event ~ 2000 years BP and supports vegetation similar to the uplands (C Burn, personal communication 2016). An ancient DTLB is located 100 m to the south of the Illisarvik basin and the Arctic Ocean is to the west of the basin, separated by a ridge of upland tundra about 50 m wide at its narrowest (Fig 1).

A vegetation survey of species presence and percent cover was done on a 50 m grid in and around the basin during the 2016 study period (Wilson, 2019). A vegetation map was created with ten units based on plant functional type and vegetation structure, with sub-units denoting sub-canopy vegetation. The unit boundaries between grid points were estimated visually by traversing the grid lines. Additional survey data on vegetation units & canopy height were collected manually with a GPS in the proximity of the EC station because greater resolution was needed for footprint modelling. Drone imagery was collected on July 23rd over two flights using a Phantom 2 drone (DJI, Shenzhen, China). The GPS points and drone imagery were used to cross reference and modify the map of Wilson et al. (2019). The ten units were then aggregated into 6 broader surface cover classes (listed from largest to smallest areal fraction within the footprint climatology): shrub, grass, sedge, upland, sparse, and water classes (Fig 1 & Table 1).

2.2 Weather and Soil Measurements

Weather data were logged on a CR1000 datalogger (Campbell Scientific Inc, Logan, UT, USA; CSI) at 5-minute intervals. A NRLite net radiometer (Kipp & Zonen, Delft, Netherlands) measured net all-wave radiation (R_n), SQ-110 quantum sensor (Apogee Instruments, Logan, UT, USA) measured photosynthetic photon flux density (*PPFD*), and a HMP35 (CSI) measured T_a and humidity (*RH*). A tipping bucket rain gauge (R.M Young Company, Travers City, MI, USA) was placed 3 m to the west of the main tripod. Soil temperature and moisture data were recorded at 30-minute intervals on CR10x dataloggers (CSI) within two soil pits with different vegetation types near the tripod: Grass (30 m to the east) and Shrub (40 m to the north). Each system measured ground heat flux (G) with custom made heat flux plates, soil temperatures (T_s) with custom made type-T thermocouples at depths of 0.08 m, and volumetric water content (θ_w) with CS616 water content reflectometers (CSI). There was one repetition of each observation per pit. The climate and soil stations operated uninterrupted from July 10th (day 192) and July 11th (day 193) respectively, until August 7th, 2016 (day 220). On July 11th and August 6th thaw depth was measured at each of the 10 chamber sites. Thaw depth was measured by inserting a graduated steel probe into the ground to point of refusal. Each site was probed five times: the median value has been used as the thaw depth at each location. Between day 193 and 197, a large herd of reindeer (500 + animals) visited Illisarvik. They mostly avoided the tripod but did graze near it on a few occasions.

https://doi.org/10.5194/bg-2019-477
Preprint. Discussion started: 12 February 2020

2.3 EC Fluxes

An EC system was placed in the southwestern portion of the basin (69° 28' 47.82", -134° 35' 18.6") and measured fluxes of CO_2 (F_{CO2}) and CH_4 (F_{CH4}) for the full study period. The EC system consisted of an open-path infrared CO_2/H_2O gas analyser (IRGA) (model LI-7500, LI-COR Inc., Lincoln, NK, USA; LI-COR), an open-path CH_4 analyser (model LI-7700, LI-COR) and a CSAT3 sonic anemometer (CSI) mounted on a tripod at a measurement height (z_m) of 3 m (Fig 2.). The EC data and air pressure (P_a) were logged at 10 Hz on the LI-7550 Analyzer Interface Unit (LI-COR). The CSAT3 was oriented to the northeast (40°) because climatology for Tuktoyaktuk indicated northerly and easterly winds are typical for July and August (Environment Canada, 2016).

Half-hourly fluxes were calculated with EddyPro V.6.2.0 (LI-COR). The software performed statistical assessments (Vickers and Mart, 1997), low and high frequency spectral corrections (Moncrieff et al., 1997 and 2004), a double rotation (Wilczak et al., 2001), applied the WPL correction to account for density fluctuations (Webb et al., 1980), and quality control (Mauder and Foken, 2004). Post processing treatments included: storage correction (calculating the net flux as the sum of the observed scalar flux and the rate of change in scalar concentration at z_m), filtering fluxes by friction velocities (u_*) below 0.1 m s^{-1}, and removing spurious half hourly measurements (Papale et al., 2006). Additionally, observations with mean winds from 220˚ ± 30˚ were removed as these to avoid uncertainties associated with the wake of the sonic anemometer, and observations were removed during precipitation events and when the open-path analyzers indicated there were any other obstructions within the path. The data were gap-filled using neural networks (NN) which have been applied to F_{CO2} and F_{CH4} in other studies (Moffat et al., 2010; Dengel et al., 2013). Details of the NN methodology are discussed in Appendix A.

The flux footprint represents the influence of upwind areas on a measured scalar flux and the footprint climatology is the average of individual footprints over a time period. Evaluation of the flux footprints and climatology help evaluate the reliability of the dataset and estimate the source area of each individual datapoint of the EC flux measurement. A scalar flux F_c sampled at $(0,0,z_m)$, can be represented as the integral of the flux footprint function *f(x,y)* and the distribution of sources/sinks (Q_c) over a domain *D* (Kljun et al., 2015):

$$F_c(0,0,z_m) = \int_D Q_c(x,y) f(x,y) \quad (1)$$

The flux contribution of upwind source areas increases sharply upwind from the measurement location to a peak then decrease gradually with increasing distance (Schmid, 2002). The empirically derived flux footprint function of Klujn et al., (2015) was used to estimate the source area of each half hourly flux measurement.

The model requires boundary layer heights which were not measured onsite. Half hourly boundary layer heights were interpolated from three-hour estimates obtained from the Global Data Assimilation System of the U.S. National Oceanic and Atmospheric Administration. The model also requires the aerodynamic roughness length (z_0) which is influenced by the canopy height and spacing. Canopy height (C_h) varied considerably within the basin (from >1 m in the north to ~0 m in the bare ground). Canopy height variability was lower in the vicinity of the EC tripod but ranged from 0.35- 0.55 m with a few taller shrubs approaching 1 m. Median z_0 was calculated for 30˚ wind sectors following Paul-Limoges et al. (2013). This calculation was performed for near neutral conditions $-0.05 \leq \frac{Zm}{L} \leq 0.05$, where

https://doi.org/10.5194/bg-2019-477
Preprint. Discussion started: 12 February 2020

L is the Obukhov length. z_0 was found to be insensitive to changes in the zero-plane displacement height, d, as $z_m >> d$, so the mean value of d around the tripod was used, where d = 2/3 C_h. Zero-plane displacement did not change significantly over the course of the study so z_0 remained fixed over the study period for each wind sector.

For each 30-minute flux observation, was solved at one-meter resolution over a 1 km^2 domain centred on the EC tripod. $f(x,y)_i$ were intersected with the surface classes to determine their relative contribution each flux observation (referred to as $Shrub_{\%}$, $Sedge_{\%}$, etc.). The footprint function is technically infinite so a fraction of each $f(x,y)_i$ was not contained within the model domain. The out-of-domain source fraction ranged from 1.8% - 4.9% with a mean of 3.2% and assumed to have minimal impact on the analysis. The half hourly flux footprints were then averaged over the study to calculate the flux footprint climatology. All post-processing and footprint modelling were carried out using Python.

2.3 Closed Chamber Measurements

In addition to EC measurements, fluxes of CO_2, CH_4, and nitrous oxide (N_2O) were sampled using a static non-steady state chamber flux technique on 11 dates between July 12 and August 5, 2016 (Laforce, 2018). Only the bare ground was a significant source of N_2O, so those results are not shown here. Chamber collars were located at ten sites, eight within and two outside the basin (Figure 1). Each surface cover class was represented by at least one chamber site, except for open water. At each site a pair of collars were installed 20 cm apart and the above ground biomass was removed from one of the collars, with the exception of the 'sparse' cover class where only one collar was installed. PVC collars 30 cm long and 24.3 cm in diameter were inserted to a depth of approximately 15 cm. The chambers were 34 cm tall and made out of polycarbonate covered in black opaque tape to maintain dark conditions inside the chamber (for more details, see Martin et al., 2018). The chambers contained a small vent (10 cm coiled 1/8" diameter copper pipe) to ensure a constant pressure during measurements. The use of opaque chambers means that F_{CO2} represents only ER. The independent estimation of ER is important as it is difficult to estimate ER using standard EC techniques at high latitude sites during Arctic summer at this latitude. Standard approaches require night-time data, a condition which was only found during a small fraction of the study period.

Measurements were made between 9:00 and 17:00 starting at a different site each day to randomize the sampling order to avoid a bias due to diurnal ranges on the 11 days when performing chamber measurements. During gas flux measurements, the chambers were sealed to the top of the collars within a groove filled with water and five 24 mL air samples were collected into evacuated 12 mL vials sealed with doubled septa. Each vial contained a small amount of magnesium perchlorate to dry the air sample. Samples were collected at 0, 5, 10, 15 and 20 minutes after the chambers were set on the collars. Air within the chamber was mixed with a 60 mL syringe attached to a three-way stopcock before each air sample was taken. Samples were stored until analysis the following fall. To monitor the integrity of the vials through shipping, storage and analysis, a number of the evacuated vials were filled with helium in the lab before the field season began.

Concentrations of CO_2, CH_4 and N_2O were determined at Carleton University, using a CP 3800 gas chromatograph (Varian Inc., Pao Alto, CA, USA) as described by Wilson and Humphreys (2010). Three replicates of five CO_2/ CH_4 standards varying from 383.1 to 15212.6 ppm CO_2 and from 1.08 to 22.11 ppm CH_4 were included in every set of

https://doi.org/10.5194/bg-2019-477
Preprint. Discussion started: 12 February 2020

measurements to create a linear relationship between gas concentration and chromatogram area. The fluxes (F_C) were calculated as follows:

$$F_C = \frac{VP}{ART}\frac{dc}{dt} \quad (2)$$

where (*dc/dt*) is the linear rate of change in the mixing ratio of the gas, *A* is the chamber area (0.0464 m^3), *V* is the chamber volume (between 0.0182 and 0.0242 m^3 adjusted for m^2 collar depth at each collar location), *R* is the ideal gas constant, *P* is pressure in *Pa* and *T* is the air temperature in Kelvin. *P* and *T* values corresponding to the time of each measurement were obtained from the EC station. Positive fluxes indicate emissions of gases to the atmosphere and negative fluxes indicate uptake by the surface. After removal of spurious point measurements (if more than 2 points were rejected, the flux measurement was rejected), *dc/dt* coefficients of determination ranged from 0.71 to 0.999. Overall, 72 vial samples were rejected out of 1135 vials and no flux measurements were rejected out of 681.

Chamber measurements were upscaled to for comparison to EC observations. ER was calculated using eq. 4 and the Q_{10} and R_{10} coefficients derived by Laforce (2018) explained in section 2.4.1. ER was calculated for each surface class separately and then weighted by footprint climatology (see Table 2). For NME, there are no standard empirical functions, so mean NME for each class was weighted by the footprint climatology instead. The weighted estimates were compared to EC observations and to help verify our findings.

2.4 Factor Selection and Gap Filling

We used an exploratory approach to identify the smallest set of factors that best predicted half hourly NEE and NME without overfitting the dataset. We started with 10 factors: four meteorological variables [(*PPFD*), T_a, vapor pressure deficit (*VPD*), wind speed (*U*)], two soil variables [volumetric water content (*VWC*) and soil temperature (T_s)], and four source area fractions [shrub (F_{Shrub}), grass (F_{Shrub}), sedge (F_{Sedge}), and upland, (F_{Upland})]. The four source area variables correspond to surface classes sampled by the chamber samples. We excluded sparse (F_{Sparse}) because its average contribution to the EC observations was only 2.1% and chamber samples indicated ER was low and NME was not significantly different from zero. A number of these variables are highly correlated but it was necessary to include them so the model could account for source area heterogeneity.

A series of neural networks (NN) were trained iteratively on bootstrapped datasets. First NN were trained on each factor individually and the one with the lowest MSE was selected. Next, NN were trained on that factor in combination with one of the remaining nine. The best performing additional factor was again selected and this process was repeated until MSE failed to improve. The most parsimonious model was identified using the one standard error (*SE*) rule. Dybowski and Roberts (2001) give the standard error of a bootstrap estimate of a given error metric (eg. $\theta = MSE$) to be

$$SE_{boot}(\theta) = \sqrt{\frac{1}{B-1}\sum_{b=1}^{B}(\theta_b - \theta_{boot})^2} \quad (3)$$

where θ_{boot} is the mean of the bootstrapped samples. The smallest set of factors where θ_{boot} was within one SE_{boot} of the minimum θ_{boot} for both NEE and NME were selected for further analysis. The models trained on those factor

https://doi.org/10.5194/bg-2019-477
Preprint. Discussion started: 12 February 2020

sets are referred to as NN_{NEE} and NN_{NME} respectively. NN modelling was done using the Keras Python library (Chollet et al., 2015), see the Appendix A for a more detailed explanation of the NN analysis.

Multiple Imputation (MI) was then used to gap fill the *NEE* and *NME* with the outputs from NN_{NEE} and NN_{NME} respectively (Vitale et al., 2018). Of the 1296 half hourly flux observations 28.9% of F_{CO2} and 31.3% of F_{CH4} were missing or filtered out. There were a few gaps in the source area fractions needed to gap-fill the flux time series because the footprint function is not valid when $u_* < 0.1$ m s^{-1}. When source area fractions were missing, they were gap-filled by using the mean source are fraction observed for winds within ± 5˚of the observed wind direction. The meteorological and soil data were continuous and did not need to be gap-filled.

2.4.1 Flux Partitioning

NEE is negative when there is uptake of CO_2 by the ecosystem and positive when there is net emission. ER and GPP are always positive, ER represents the sum of heterotrophic and autotrophic respiration and GPP represents photosynthetic uptake of CO_2. Night-time NEE observations (eg. *PPFD* <= 10 µmol m^{-2} s^{-1}) are typically used to quantify ER because GPP ~ 0 (Aubinet et al., 2012). Some NN analyses of NEE have trained separate models for night-time and daytime conditions (Papale & Valenini, 2003). However, these methods are not practical during the Arcitc summer, the sun did not set at Illisarvik until July 28th, over half way through the study period. There were not enough night-time samples (n=100) to be worth training a separate NN. Instead, we estimated ER by calculating the intercept of NN_{NEE} at PPFD = 0 µmol m^{-2} s^{-1} for all observations. This estimate is referred to as NN_{ER}. Laforce (2018) fit a Q_{10} equation to the chamber ER observations:

$$ER = R_{10} Q_{10}^{\frac{(T_a - 10)}{10}} \quad (4)$$

where R_{10} is the base respiration at 10 C˚ and Q_{10} is the temperature sensitivity coefficient. We fit the night-time EC observations available (n=100) to this Q_{10} equation for comparison (Aubinet et al., 2012).

2.4.1 Factor Analysis and Upscaling

The trained NNs were used to investigate how individual factors influenced NEE and NME. The partial first derivative of the model response to one controlling factor was calculated while keeping all other inputs fixed. For example, the partial first derivative, $\frac{\partial NEE}{\partial \mathrm{PPFD}}$, is an approximation of the NEE light response curve under a specific set of conditions. Similarly, NN_{NME} can be used to approximate NME response to controls like *VWC* or T_s. For both fluxes, the selected model contained at least one source area fraction variable, indicating the vegetation type(s) which had significant influence over both NEE and NME. We mapped NN_{NEE} and NN_{NME} to full coverage for the surface classes to approximate their fluxes and compare with the chamber observations.

3 Results & Discussion

During the 29-day study, half-hourly T_a and T_s ranged between 0.4 and 26.2 C˚ and 4.4 and 11.0 C˚, respectively (Fig 2a). Day length and maximum solar altitude decreased from 24 hours to 19.25 hours and 41.6˚ to 35.4˚, but daily

https://doi.org/10.5194/bg-2019-477
Preprint. Discussion started: 12 February 2020

PPFD was more influenced by variations in cloud cover. Precipitation (19 mm) fell on 14 of the 28 days with trace snowfall on three of those days, but *VWC* decreased throughout the period (Fig 2b). At the onset of the study period, *VWC* was high and soils were saturated with ponding in the sedge areas. By the end of the study most of this surface water had dried up. On July 11th average thaw depth (cm) was 37, 45, 51, 64, 81 at upland, sedge, grass, shrub, and sparse classes, respectively. By August 6th, average thaw depth was 45, 62 and 66 cm at upland, sedge and grass surface classes and over 100 cm at both the shrub and sparse classes.

A strong low-pressure system stalled off the coast between day of year (DOY) 199 and 204. This caused westerly winds to occur much more frequently than is typical for July and August. The 50%, 80% and 90% flux footprint climatology contours are shown in Fig 1a. Mean source area fractions indicate the EC observations were skewed towards the grass surface class and under-sampled the shrub class, but the range of surface classes sampled was diverse enough to allow for testing of the impact of source area fraction on the fluxes (Table 2).

3.1 EC & Chamber Observations

EC observations indicate that the flux footprint area was a carbon sink during the peak growing season, but fluxes varied considerably from day to day. Gap-filled daily NEE ranged from -3.7 to -0.2 g C-CO_2 m^{-2} d^{-1} with a mean -1.5 [$CI_{95\%}$ ± 0.2] g C-CO_2 m^{-2} d^{-1} (Figure 2c). Estimated ER was 2.2 [$CI_{95\%}$ ± 0.9] g C-CO_2 m^{-2} d^{-1} with corresponding GPP 3.7 g C-CO_2 m^{-2} d^{-1}. There were no notable trends in NEE or ER over the study period. Our observations are within ranges observed from young DTLB on the Barrow Peninsula. NEE was greater than (ie. less carbon uptake) EC observations of from four wetter, sedge dominated DTLB, where peak season NEE was -2.5 g C-CO_2 m^{-2} d^{-1}, ER (1.5 g C-CO_2 m^{-2} d^{-1}) was lower than at Illisarvik while GPP (4.0 g C-CO_2 m^{-2} d^{-1}) was slightly higher (Zona et al., 2010). But NEE was less than (ie. more carbon uptake) upscaled chamber estimates for wet meadow DTLB (-0.9 g C-CO_2 m^{-2} d^{-1}), while ER (2.7 g C-CO_2 m^{-2} d^{-}) and GPP (3.5 g C-CO_2 m^{-2} d^{-}) were higher and lower than Illisarvik (Lara et al., 2015). Mid-day NEE at was comparable to aircraft observations from young DTLB (Zulueta et al., 2011). Gap-filled daily NME was modest, ranging from 2.0 to 25.1 mg C-CH_4 m^{-2} d^{-1} with a mean of 8.7 [$CI_{95\%}$ ± 0.4] mg C-CH_4 m^{-2} d^{-1} (Fig 3d). Even accounting for the greater GWP of CH_4, NME did not constitute a significant component of the carbon balance. Daily NME decreased over the study period as soils in the basin dried. NME at Illisarvik was much less than EC observations from in a wet sedge dominated DTLB (18.4 mg C-CH_4 m^{-2} d^{-1}) and chamber observations from DTLB (26.1 mg C-CH_4 m^{-2} d^{-}) on the Barrow Peninsula (Zona et al., 2009; Lara et al., 2015). Chamber ER was higher than EC estimates and showed modest variability among vegetation classes (Fig 3a). Greatest ER was observed in the Sedge, Upland, and Grass classes where fluxes were very similar at 5.5 [$CI_{95\%}$ ± 1.2], 5.4 [$CI_{95\%}$ ± 1.2] and 4.9 [$CI_{95\%}$ ± 0.7] g C-CO_2 m^{-2} d^{-1}, Shrub was significantly less (3.5 [$CI_{95\%}$ ± 0.6] g C-CO_2 m^{-2} d^{-1}) than the other vegetated classes and Sparse had the lowest ER (2.0 [$CI_{95\%}$ ± 0.3] g C-CO_2 m^{-2} d^{-1}). These values were generally higher than chamber observations from DTLB or tundra sampled by Lara et al. (2015). Q_{10} and R_{10} differed between vegetation classes, Sedge were the most sensitive to changes in air temperature, while Upland had the highest base respiration (Table 3). EC estimated Q_{10} and R_{10} (r^2 = 0.47) were generally lower than the vegetated chambers, but most similar to Shrub, which was the largest component of the footprint.

https://doi.org/10.5194/bg-2019-477
Preprint. Discussion started: 12 February 2020

Chamber NME was much smaller than ER but there was significantly more variability among vegetation classes (Fig 3b). Sedge was a very strong CH_4 source at 114.7 [$CI_{95\%}$ ± 15.3] mg C-CH_4 m^{-2} d^{-1}, which is comparable to chamber observations from vegetated ponds on the Barrow Peninsula (Lara et al., 2015). Sites across the arctic with sedges have higher NME than sites without sedges (Olefeldt et al., 2013). Shrub and Grass were very weak sources, 0.7 [$CI_{95\%}$ ± 0.3] and 0.4 [$CI_{95\%}$ ± 0.3] mg C-CH_4 m^{-2} d^{-1}, respectively and Sparse was neutral. Upland was a net sink for CH_4 -1.1 [$CI_{95\%}$ ± 0.4] mg C-CH_4 m^{-2} d^{-1}. Lara et al. (2015) did not find upland areas on the Barrow Peninsula to be CH_4 sinks, but upland tundra is known to be a globally significant methane sink (Whalen and Reedburgh, 1990; Whalen et al., 1996) Upland fluxes were negatively correlated with T_s, Sparse and Grass had no clear relationships, while Shrub and Sedge had significant positive correlations with *VWC* and T_s, but there were no straightforward empirical functions to model NME like there is for ER.

Footprint scaled chamber estimates of ER and NME were about 32% and 31% greater than the EC estimates. Mean estimated ER estimated was 3.2 g C-CO_2 m^{-2} d^{-1} and NME was 12.9 [$CI_{95\%}$ ± 8.1] mg C-CH_4 m^{-2} d^{-1} The discrepancies between the EC and chamber observations is often observed and has been attributed to differences in measurement techniques, the small sample size of chamber observations, and sampling bias since all chamber measurements were taken during the day with fair weather (Katayanagi et al., 2005; Chaichana et al., 2018). Meijide et al. (2011) found that chamber NEE could be up to twice as large as EC observations and Riederer et al. (2014) also found chamber NME estimates were about 30% higher than EC estimates.

3.2 NEE Response to Environmental Factors and Vegetation Type

NN_{NEE} (r^2 = 0.91) had four factors: *PPFD*, *VPD*, *VWC*, and *Shrub*. For comparison, NEE estimated using the Q_{10} paired with a light response curve (r^2 = 0.8) or a random forest regression tree (r^2 = 0.86) trained with the factors selected by NN_{NEE} were not as accurate as NN_{NEE}. *PPFD* is the primary control over NEE, a NN trained on *PPFD* alone provided a reasonable fit (r^2 = 0.83). The three additional factors: *VPD*, *VWC*, and *Shrub*, helped NN_{NEE} fit a wider variety of conditions. Looking at the partial first derivative of NN_{NEE} under different conditions, we can inspect the modelled light response curves (α). The minimum of α is the peak light use efficiency. With increasing *PPFD*, light use becomes less efficient and α approaches zeros as the light response nears saturation.

VPD was a secondary control over NEE, which is consistent with the findings of another study using NN to analyse NEE (Moffat et al., 2012). Increasing *VPD* increased peak light use efficiency and net C uptake until a threshold, above which it had a strong limiting effect (fig 4a & b). For example, under dry conditions (eg. VPD = 1500 Pa), peak light use is less efficient (-12 nmol CO_2 μmol^{-1} photon) than under optimal conditions (-18 nmol CO_2 μmol^{-1} photon). The value of this threshold was dependent upon soil moisture: from 1000 pa when *VWC* was highest to 200 pa when *VWC* was low.

Mapping NN_{NEE} and NN_{ER} at $Shrub_{\%}$ = 100%, $Shrub_{\%}$ = 0%, and $Shrub_{\%}$ = 36% (footprint climatology), shows that *VWC* and $Shrub_{\%}$ were the primary controls over ER and thus influenced NEE (fig 4c & d). We can see from the partial first derivates of NN_{ER} that increasing *VWC* increases ER from shrub areas. In the absence of shrubs, increasing VWC inhibits ER. The partial first derivative of NN_{NEE} shows that *VWC* slightly limits NEE from non-Shrub areas and significantly reduces it in Shrub areas. The *VWC* relationships support Zona et al. (2010) who found *VWC*

https://doi.org/10.5194/bg-2019-477
Preprint. Discussion started: 12 February 2020

explained 70% of the variability in daily peak season NEE and ER and Kittler et al. (2016) who found drier soils increased both NEE after a wet tundra drainage experiment in Siberia. The chamber data supports the inclusion of $Shrub_{\%}$ because Shrub ER was significantly lower than the other vegetation classes.

3.3 NME Response to Environmental Factors and Vegetation Type

NN_{NME} (r^2 = 0.62) had five factors: $Sedge_{\%}$, $Shrub_{\%}$ *VWC*, T_S, *VPD*, and *U*. A random forest regression tree (r^2 = 0.51) and a GLM (r^2 = 0.25) trained on the factors selected by NN_{NME} were not as accurate as NN_{NME}. NME was more chaotic and less dependent on any one factor than NEE which is why the NN_{NME} needed an extra factor and had a lower r^2 score. Source area had a significant effect on NME, and it is encouraging that the model contains $Sedge_{\%}$ and $Shrub_{\%}$ since Sedge and Shrub were the strongest CH_4 source and largest footprint component respectively. These two factors can combine to map NME under three general situations: we can extrapolate to $Sedge_{\%}$ = 100 % & $Shrub_{\%}$ = 0 % or $Sedge_{\%}$ = 0 % & $Shrub_{\%}$ 100 %, or to footprint climatology (Table 2). The footprint climatology means that some upland tundra is also included in the estimate, which brings NME down.

VWC was the primary climatic driver identified by NN_{NME}. Wetter soils had a consistent positive effect on NME which was strongest when $Sedge_{\%}$ was high (Fig 5a & b). Between driest and wettest conditions, estimated NME increased: by an order of magnitude at $Sedge_{\%}$ = 100 %, 4-fold at $Shrub_{\%}$ = 100%, and from neutral to a source at footprint climatology. The effect of soil moisture on CH_4 production and emission has been noted in many other studies (e.g. Zona et al., 2009; Nadeau et al., 2013; Olefeldt et al., 2013).

Higher T_s generally had a negative effect on NME (Fig 5c & d). Higher soil temperatures increase the oxidation potential of methanotrophs (Liu et al., 2016; King and Adamsen, 1992), so this result was expected for the drier portions of the basin and upland tundra. However, this wasn't expected for the sedge areas because most studies find NME in sedges is positively correlated to T_s (Olefeldt et al., 2013). There was diurnal cycle in NME with NME peaking in the morning when T_s was at its daily minimum, which supports this finding. NN_{NME} performance improved less with the addition of *U* indicating the NN_{NME} was near saturation and its effects are less relevant. Higher wind speed had a weak limiting effect on NME when VWC was high and increased NME when VWC was low (not shown). High winds were mainly associated with two strong storm events. In order to better resolve this relationship a longer dataset would be needed.

3.4 Future Trajectories

Presently, NEE and ER at Illisarvik are within ranges observed within similar landscape features on the Barrow Peninsula but NME was considerably lower. However, Illisarvik will continue to evolve and the trajectory it takes could significantly alter the carbon balance. Most DTLB on Richards Island and the Tuktoyaktuk Peninsula evolve into wet sedge-moss peatlands (Ovendend, 1986). As do DTLB on the Barrow Peninsula (Lara et al., 2015). This would cause NME to increase significantly. NN_{NME} estimated that at $Sedge_{\%}$ = 100% mean NME would be 17.9 [$CI_{95\%}$ ± 10.6] mg C-CH_4 m^{-2} d^{-1}, which is comparable to EC observations from a wet sedge DTLB on the Barrow Peninsula (Zona et al., 2009). If the basin becomes wetter and the shrubs are displaced by sedges and grasses net

https://doi.org/10.5194/bg-2019-477
Preprint. Discussion started: 12 February 2020

carbon uptake may increase. NN_{NEE} and NN_{ER} estimated that at $Shrub_{\%}$ = 0% NEE and ER over the study period would be -1.9 [$CI_{95\%}$ ± 0.5] g C-CO_2 m^{-2} d^{-1} and 1.8 [$CI_{95\%}$ ± 1.1] g C-CO_2 m^{-2} d^{-1} respectively.

However, active maintenance of the basin's outlet channel (C. Burn, personal communication 2016) has artificially lowered soil moisture and potentially limited this transition. This coupled with climate change will promote shrub expansion and Illisarvik could end up more like the shrub dominated DTLB of Old Crow Flats, Yukon (Lantz et al., 2015). NN_{NEE} and NN_{ER} estimated that at $Shrub_{\%}$ = 100% NEE and ER over the study period would be -0.9 [$CI_{95\%}$ ± 1.5] g C-CO_2 m^{-2} d^{-1} and 2.4 [$CI_{95\%}$ ± 1.6] g C-CO_2 m^{-2} d^{-1} respectively. Other studies have also suggested that shrub expansion could influence NEE by increasing ER (Merbould et al., 2009; Meyer-Smith et al., 2011). NN_{NME} estimated NME would be 13.1 [$CI_{95\%}$ ± 9.4] mg C-CH_4 m^{-2} d^{-1} at $Shrub_{\%}$ = 100%, meaning the basin will likely remain a net source of CH_4.

4 Conclusions

This study investigated NEE, ER and NME in the Illisarvik DTLB using EC and chamber data. To our knowledge this is the first such study conducted in a DTLB outside of the Barrow Peninsula. Our observations were generally in agreement with other studies but show how Illisarvik differs from the colder, wetter DTLB on the Barrow Peninsula. Illisarvik is a carbon sink during the growing season with NME only having a small positive effect on the net carbon balance. Illisarvik NEE was similar to young DTLB on the Barrow Peninsula, while NME was lower due to better drainage, drier conditions, and more diverse vegetation. However, higher NME in early July indicated we likely missed a key period of CH_4 emissions earlier in the season. A longer, more comprehensive study would be needed to resolve the annual carbon budget for Illisarvik.

Chamber measurements of ER and NME from different land cover classes within and outside the basin added context to the EC observations. Vegetation class (and associated difference in terrain and soil properties) had only a slight impact on NEE and ER but was one of the dominant controls over NME. Sedge areas were a strong source of CH_4, other vegetation types in the basin were weak sources, and upland areas were a net sink. These results suggest that NME in particular is expected to shift as both the terrain and the vegetation of the Illisarvik DTLB continues to evolve.

Appendix A: Neural Networks analysis and uncertainty calculations

Typically, NEE is gap-filled using flux-partitioning algorithms that model ER and GPP separately using T_S and *PPFD*, respectively (e.g. Lee et al., 2017; Aubinet, 2012). However, this method requires night-time observations and thus does not perform well for Arctic summertime measurements due to the limited number of samples available during low light conditions. There are no widely agreed upon functional relationships for gap-filling NME since CH_4 production and consumption vary considerably both between different landcover types and environmental conditions. Some methods that have been used include classification and regression trees (CART) (Nadeau et al., 2013; Sachs et al., 2008), general linear models (GLM) (Zona et al., 2009), and mean diurnal variation (Nadeau et al., 2014). We attempted to use a GLM, CART, and random forest regression trees but they were not flexible enough to account for source area variability.

https://doi.org/10.5194/bg-2019-477
Preprint. Discussion started: 12 February 2020

Neural networks (NN) are flexible machine learning methods that are ideally suited to perform non-linear, multivariate regression. They make no a priori assumptions about the functional relationships between the factors and responses. (Melesse and Hanley, 2005; Desai et al., 2008). NN are universal approximators; given enough hidden nodes a NN is capable of mapping any continuous function to an arbitrary degree of accuracy (Hornik et al., 1991). If all relevant climate and ecosystem information are available to a network, the remaining variability can be attributed to noise in the measurement (Moffat et al., 2010).

NN have been shown to be among the best performing methods for gap-filling NEE data for forest sites in Europe (Moffat et al., 2007). They have also been used to gap-fill NME time series in sub-arctic wetlands, tundra sites, and wet sedge tundra (Dengel et al., 2013). NN have been used to identify and model factors influencing NEE and to partition NEE into ER and GPP (Moffat et al., 2010). NNs have even been used to upscale fluxes from the ecosystem level to the continental scale (Dou and Yang, 2018; Papale et al, 2003).

A NN approximates a true regression function $F(X)$:

$$F(X) = t(X) - \varepsilon(X) \quad \text{(A1)}$$

where $t(X)$ is the target function and $\varepsilon(X)$ the noise (Khosravi and Nahavandi, 2010). $X = [x_0, x_1, \dots, x_M]$ where $x_0 = 1$ is a bias term and $[x_1, \dots, x_M]$ are the independent variables. M denotes the number of independent variables. The network approximates $F(X)$ as $f(X, w)$ by mapping the relationship between X and the target. Here we used feed-forward dense NN with a single hidden layer:

$$f(X, w) = \sum_{h=1}^{H} \beta_h g\left(\sum_{m=0}^{M} \gamma_{hm} x_m\right) \quad \text{(A2)}$$

$g(\cdot)$ is a non-linear transfer function, here we used the rectified linear activation unit (ReLu) (Anders and Korn, 1999). H denotes the number of hidden nodes in the network and must be assigned before training. Too many hidden nodes and the NN will overfit the training data, too few and it will underfit. Early stopping will prevent NN from overfitting training sets (Weigend, 1993; Sarle, 1995; Tetko et al., 1995). Therefore, it is more important to ensure a NN has enough hidden nodes to adequately map the target function (Smith, 1994). We set H to a function M, the number of training samples (N), and the number of targets (1):

$$H = \frac{N}{a*(M+1)} \quad \text{(A3)}$$

This rule of thumb ensures a NN has sufficient flexibility to approximate the target response. The weights $w = [\beta_1 \dots \beta_N, \gamma_{10} \dots \gamma_{NM}]$ are randomly initialized and after each model iteration is updated by backpropagating the error through the network. N denotes the number of observations or targets. The error metric most commonly used is the mean squared error, MSE:

$$MSE = \sum_{i=1}^{N} (f(X_i) - t_i)^2 \quad \text{(A4)}$$

The weights are adjusted in the direction that will decrease the error and training continues until a stopping criterion is reached. We chose to set aside 20% of the training data as a test set to be used for early stopping, and terminated training when the MSE of the test set failed to improve for 10 consecutive iterations.

Bootstrapping is used to account for model variability and estimate confidence and prediction intervals by training NN on B different realizations of the dataset, where B is the number of bootstrapped samples, we used $B = 30$ (Heskes, 1997; Khosravi & Nahavandi, 2010). An individual NN generates point outputs approximating a target function with no information on the confidence in those estimates (Khosravi & Nahavandi, 2010). However, there are usually

https://doi.org/10.5194/bg-2019-477
Preprint. Discussion started: 12 February 2020

multiple $f(X,w)$ that approximate $F(X)$ because of the random weight initializations (Weigend & LeBaron, 1994). As such, there are two sources of error we are concerned with, the accuracy of our estimation of $F(X)$ and the accuracy of our estimates with respect to the target. A confidence interval describes the first (e.g. $F(X) - f(X,w)$) while a prediction interval describes the latter (eg. $t(X) - f(X,w)$) (Heskes, 1997). By definition, a prediction interval contains the confidence interval because:

$$t(X) - f(X,w) = [F(X) - f(X,w)] + \varepsilon(X) \quad \text{(A5)}$$

For b = 1 … *B*, a random sample with replacement of size *p* is drawn from the original dataset. Setting *p* equal to the size of the original dataset yields a set of *B* training sets each containing approximately 67% of the original dataset. The 33% leftover from each bootstrap sampled can be used for model validation (Heskes, 1997). The average of our ensemble of networks can then serve as our approximation of F(*X*):

$$F(X) = \frac{1}{B}\sum_{b=1}^{B} f_b(X,W) \quad \text{(A6)}$$

The variance of the model outputs is:

$$\sigma^2(X) = \frac{1}{B-1}\sum_{b=1}^{B}\left(f_b(X,W) - F(X)\right)^2 \quad \text{(A7)}$$

A confidence interval (CI) for $F(X)$ can be calculated as $F(X) \pm t_{(1-\propto,df)}\sigma(X)$, where *tscore* is the students t-score, 1-α is the desired confidence level, and df are the degrees of freedom which are set to the number of bootstrapped samples B. NN performance can be seen to improve with the inclusion of more factors, until the model saturates and becomes over-parametrized (Figure A1).

Data & Code availability

Our data and code are available on github: https://github.com/June-Spaceboots/Illisarvik_CFluxes

Author Contribution

JS, AC, and GH designed the EC study. AL and EH designed the chamber study. JS collected, processed, and analysed the EC data. AL and EH collected the chamber data with help from JS. AL and EH processed the chamber data. JS designed and conducted the NN analysis. JS prepared the manuscript with help from the co-authors

Competing interests

The authors declare they have no competing interests.

Acknowledgements

We would like to thank: the staff at the Aurora Research Institute in Inuvik for providing logistical support, Chris Burn for allowing us to work at Illisarvik and the knowledge he shared, Alice Wilson for sharing vegetation survey

https://doi.org/10.5194/bg-2019-477
Preprint. Discussion started: 12 February 2020

data, and Tony Lekowicz for collecting and sharing the drone images. Funding for this study was provided by the Canada Foundation for Innovation and the National Science and Engineering Research Council (NSERC).

References

Anders, U. and Korn, O.: Model selection in neural networks, Neural Networks, 12(2), 309–323, doi:10.1016/S0893-6080(98)00117-8, 1999.

Aubinet, M., Vesala, T. and Papale, D., Eds.: Eddy Covariance: A Practical Guide to Measurement and Data Analysis, 2012 edition., Springer, Dordrecht ; New York., 2012.

Billings, W. and Peterson, K.: Vegetational Change and Ice-Wedge Polygons Through the Thaw-Lake Cycle, Arctic and Alpine Research, 12(4), 413–432, doi:10.2307/1550492, 1980.

Canada, E. and C. C.: Canadian Climate Normals - Climate - Environment and Climate Change Canada, [online] Available from: https://climate.weather.gc.ca/climate_normals/index_e.html (Accessed 3 December 2019), 2011.

Chaichana, N., Bellingrath-Kimura, S. D., Komiya, S., Fujii, Y., Noborio, K., Dietrich, O. and Pakoktom, T.: Comparison of Closed Chamber and Eddy Covariance Methods to Improve the Understanding of Methane Fluxes from Rice Paddy Fields in Japan, Atmosphere, 9(9), 356, doi:10.3390/atmos9090356, 2018.

Chollet, F. and others: Keras, [online] Available from: https://keras.io, 2015.

Dengel, S., Zona, D., Sachs, T., Aurela, M., Jammet, M., Parmentier, F. J. W., Oechel, W. and Vesala, T.: Testing the applicability of neural networks as a gap-filling method using CH₄ flux data from high latitude wetlands, Biogeosciences, 10(12), 8185–8200, doi:10.5194/bg-10-8185-2013, 2013.

Desai, A. R., Richardson, A. D., Moffat, A. M., Kattge, J., Hollinger, D. Y., Barr, A., Falge, E., Noormets, A., Papale, D., Reichstein, M. and Stauch, V. J.: Cross-site evaluation of eddy covariance GPP and RE decomposition techniques, Agricultural and Forest Meteorology, 148(6), 821–838, doi:10.1016/j.agrformet.2007.11.012, 2008.

Dou, X. and Yang, Y.: Estimating forest carbon fluxes using four different data-driven techniques based on long-term eddy covariance measurements: Model comparison and evaluation, Science of The Total Environment, 627, 78–94, doi:10.1016/j.scitotenv.2018.01.202, 2018.

Dybowski, R. and Roberts, S. J.: Confidence intervals and prediction intervals for feed-forward neural networks, Clinical applications of artificial neural networks, 298–326, 2001.

Foken, T., Göockede, M., Mauder, M., Mahrt, L., Amiro, B. and Munger, W.: Post-Field Data Quality Control, in Handbook of Micrometeorology, edited by X. Lee, W. Massman, and B. Law, pp. 181–208, Springer Netherlands., 2004.

French, H. M.: The Periglacial Environment, John Wiley & Sons., 2013.

Heskes, T.: Practical Confidence and Prediction Intervals, in Advances in Neural Information Processing Systems 9, pp. 176–182, MIT press., 1997.

Hornik, K.: Approximation capabilities of multilayer feedforward networks, Neural networks, 4(2), 251–257, 1991.

van Huissteden, J., Berrittella, C., Parmentier, F. J. W., Mi, Y., Maximov, T. C. and Dolman, A. J.: Methane emissions from permafrost thaw lakes limited by lake drainage, Nature Clim. Change, 1(2), 119–123, doi:10.1038/nclimate1101, 2011.

https://doi.org/10.5194/bg-2019-477
Preprint. Discussion started: 12 February 2020

Jones, B. M., Grosse, G., Arp, C. D., Jones, M. C., Anthony, K. M. W. and Romanovsky, V. E.: Modern thermokarst lake dynamics in the continuous permafrost zone, northern Seward Peninsula, Alaska, Journal of Geophysical Research: Biogeosciences, doi:10.1029/2011JG001666@10.1002/(ISSN)2169-8961.TKLCARBON1, 2018.

Katayanagi, N.: Spatial variability of greenhouse gas fluxes from soils of various land uses on a livestock farm in southern Hokkaido, Japan, Phyton (Austria) Special Issue:" APGC 2004", 45, 309–318, 2005.

Khosravi, A. and Nahavandi, S.: A Comprehensive Review of Neural Network-based Prediction Intervals and New Advances, , 17, 2010.

King, G. M. and Adamsen, A. P. S.: Effects of Temperature on Methane Consumption in a Forest Soil and in Pure Cultures of the Methanotroph Methylomonas rubra, Appl. Environ. Microbiol., 58(9), 2758–2763, 1992.

Kittler, F., Burjack, I., Corradi, C. A. R., Heimann, M., Kolle, O., Merbold, L., Zimov, N., Zimov, S. and Gockede, M.: Impacts of a decadal drainage disturbance on surface-atmosphere fluxes of carbon dioxide in a permafrost ecosystem, Biogeosciences, 13(18), 5315–5332, doi:10.5194/bg-13-5315-2016, 2016.

Kljun, N., Calanca, P., Rotach, M. W. and Schmid, H. P.: A simple two-dimensional parameterisation for Flux Footprint Prediction (FFP), Geoscientific Model Development, 8(11), 3695–3713, 2015.

Lantz, T. C. and Turner, K. W.: Changes in lake area in response to thermokarst processes and climate in Old Crow Flats, Yukon, J. Geophys. Res.-Biogeosci., 120(3), 513–524, doi:10.1002/2014JG002744, 2015.

Lara, M. J., McGuire, A. D., Euskirchen, E. S., Tweedie, C. E., Hinkel, K. M., Skurikhin, A. N., Romanovsky, V. E., Grosse, G., Bolton, W. R. and Genet, H.: Polygonal tundra geomorphological change in response to warming alters future CO2 and CH4 flux on the Barrow Peninsula, Global Change Biology, 21(4), 1634–1651, doi:10.1111/gcb.12757, 2015.

Lee, S.-C., Christen, A., Black, A. T., Johnson, M. S., Jassal, R. S., Ketler, R., Nesic, Z. and Merkens, M.: Annual greenhouse gas budget for a bog ecosystem undergoing restoration by rewetting, Biogeosciences, 14(11), 2799–2814, doi:10.5194/bg-14-2799-2017, 2017.

Liu, Y., Liu, X., Cheng, K., Li, L., Zhang, X., Zheng, J., Zheng, J. and Pan, G.: Responses of Methanogenic and Methanotrophic Communities to Elevated Atmospheric CO2 and Temperature in a Paddy Field, Front Microbiol, 7, doi:10.3389/fmicb.2016.01895, 2016.

Mackay, J., R.: An experiment in lake drainage, Richards Island, Northwest Territories: a progress report., Geological Survey of Canada, Paper, (81–1A:), 63–68, 1981.

Mackay, J. R.: Periglacial features developed on the exposed lake bottoms of seven lakes that drained rapidly after 1950, Tuktoyaktuk Peninsula area, western Arctic coast, Canada, Permafrost Periglacial Process., 10(1), 39–63, doi:10.1002/(SICI)1099-1530(199901/03)10:1<39::AID-PPP305>3.3.CO;2-I, 1999.

Mackay, J. R. and Burn, C. R.: The first 20 years (1978-1979 to 1998-1999) of active-layer development, Illisarvik experimental drained lake site, western Arctic coast, Canada, Can. J. Earth Sci., 39(11), 1657–1674, doi:10.1139/E02-068, 2002.

Marsh, P., Russell, M., Pohl, S., Haywood, H. and Onclin, C.: Changes in thaw lake drainage in the Western Canadian Arctic from 1950 to 2000, Hydrol. Process., 23(1), 145–158, doi:10.1002/hyp.7179, 2009.

https://doi.org/10.5194/bg-2019-477
Preprint. Discussion started: 12 February 2020

Martin, A. F., Lantz, T. C. and Humphreys, E. R.: Ice wedge degradation and CO2 and CH4 emissions in the Tuktoyaktuk Coastlands, Northwest Territories, Arctic Science, 4(1), 130–145, 2017.

Mauder, M. and Foken, T.: Documentation and Instruction Manual of the Eddy Covariance Software Package TK2, Univ., Abt. Mikrometeorologie., 2004.

Meijide, A., Manca, G., Goded, I., Magliulo, V., Tommasi, P. di, Seufert, G. and Cescatti, A.: Seasonal trends and environmental controls of methane emissions in a rice paddy field in Northern Italy, Biogeosciences, 8(12), 3809–3821, doi:https://doi.org/10.5194/bg-8-3809-2011, 2011.

Melesse, A. M. and Hanley, R. S.: Artificial neural network application for multi-ecosystem carbon flux simulation, Ecological Modelling, 189(3), 305–314, doi:10.1016/j.ecolmodel.2005.03.014, 2005.

Merbold, L., Kutsch, W. L., Corradi, C., Kolle, O., Rebmann, C., Stoy, P. C., Zimov, S. A. and Schulze, E.-D.: Artificial drainage and associated carbon fluxes (CO2/CH4) in a tundra ecosystem, Global Change Biology, 15(11), 2599–2614, doi:10.1111/j.1365-2486.2009.01962.x, 2009.

Moffat, A. M., Papale, D., Reichstein, M., Hollinger, D. Y., Richardson, A. D., Barr, A. G., Beckstein, C., Braswell, B. H., Churkina, G., Desai, A. R., Falge, E., Gove, J. H., Heimann, M., Hui, D., Jarvis, A. J., Kattge, J., Noormets, A. and Stauch, V. J.: Comprehensive comparison of gap-filling techniques for eddy covariance net carbon fluxes, Agricultural and Forest Meteorology, 147(3–4), 209–232, doi:10.1016/j.agrformet.2007.08.011, 2007.

Moffat, A. M., Beckstein, C., Churkina, G., Mund, M. and Heimann, M.: Characterization of ecosystem responses to climatic controls using artificial neural networks, Global Change Biology, 16(10), 2737–2749, doi:10.1111/j.1365-2486.2010.02171.x, 2010.

Moncrieff, J., Clement, R., Finnigan, J. and Meyers, T.: Averaging, Detrending, and Filtering of Eddy Covariance Time Series, in Handbook of Micrometeorology, edited by X. Lee, W. Massman, and B. Law, pp. 7–31, Springer Netherlands., 2004.

Moncrieff, J. B., Massheder, J. M., de Bruin, H., Elbers, J., Friborg, T., Heusinkveld, B., Kabat, P., Scott, S., Soegaard, H. and Verhoef, A.: A system to measure surface fluxes of momentum, sensible heat, water vapour and carbon dioxide, Journal of Hydrology, 188, 589–611, doi:10.1016/S0022-1694(96)03194-0, 1997.

Myers-Smith, I. H., Forbes, B. C., Wilmking, M., Hallinger, M., Lantz, T., Blok, D., Tape, K. D., Macias-Fauria, M., Sass-Klaassen, U., Lévesque, E., Boudreau, S., Ropars, P., Hermanutz, L., Trant, A., Collier, L. S., Weijers, S., Rozema, J., Rayback, S. A., Schmidt, N. M., Schaepman-Strub, G., Wipf, S., Rixen, C., Ménard, C. B., Venn, S., Goetz, S., Andreu-Hayles, L., Elmendorf, S., Ravolainen, V., Welker, J., Grogan, P., Epstein, H. E. and Hik, D. S.: Shrub expansion in tundra ecosystems: dynamics, impacts and research priorities, Environ. Res. Lett., 6(4), 045509, doi:10.1088/1748-9326/6/4/045509, 2011.

Nadeau, D. F., Rousseau, A. N., Coursolle, C., Margolis, H. A. and Parlange, M. B.: Summer methane fluxes from a boreal bog in northern Quebec, Canada, using eddy covariance measurements, Atmospheric Environment, 81, 464–474, doi:10.1016/j.atmosenv.2013.09.044, 2013.

Olefeldt, D., Turetsky, M. R., Crill, P. M. and McGuire, A. D.: Environmental and physical controls on northern terrestrial methane emissions across permafrost zones, Glob Change Biol, 19(2), 589–603, doi:10.1111/gcb.12071, 2013.

https://doi.org/10.5194/bg-2019-477
Preprint. Discussion started: 12 February 2020

O'Neill, H. B., Burn, C. R. and Gajewski, K.: Physical and temporal factors controlling the development of near-surface ground ice at Illisarvik, western Arctic coast, Canada, Canadian Journal of Earth Sciences, 49(9), 1096–1110, 2012.

Ovenden, L.: Vegetation Colonizing the Bed of a Recently Drained Thermokarst Lake (illisarvik), Northwest-Territories, Can. J. Bot.-Rev. Can. Bot., 64(11), 2688–2692, 1986.

Papale, D. and Valentini, R.: A new assessment of European forests carbon exchanges by eddy fluxes and artificial neural network spatialization, Global Change Biology, 9(4), 525–535, doi:10.1046/j.1365-2486.2003.00609.x, 2003.

Papale, D., Reichstein, M., Aubinet, M., Canfora, E., Bernhofer, C., Kutsch, W., Longdoz, B., Rambal, S., Valentini, R., Vesala, T. and others: Towards a standardized processing of Net Ecosystem Exchange measured with eddy covariance technique: algorithms and uncertainty estimation, Biogeosciences, 3(4), 571–583, 2006.

Paul-Limoges, E., Christen, A., Coops, N., Black, T. and Trofymow, J.: Estimation of aerodynamic roughness of a harvested Douglas-fir forest using airborne LiDAR, Remote Sensing of Environment, 136, 225–233, doi:10.1016/j.rse.2013.05.007, 2013.

Riederer, M., Serafimovich, A. and Foken, T.: Net ecosystem CO2 exchange measurements by the closed chamber method and the eddy covariance technique and their dependence on atmospheric conditions, Atmospheric Measurement Techniques, 7(4), 1057–1064, doi:https://doi.org/10.5194/amt-7-1057-2014, 2014.

Sachs, T., Wille, C., Boike, J. and Kutzbach, L.: Environmental controls on ecosystem-scale CH4 emission from polygonal tundra in the Lena River Delta, Siberia, Journal of Geophysical Research-Biogeosciences, 113, G00A03, doi:10.1029/2007JG000505, 2008.

Sarle, W. S.: Stopped Training and Other Remedies for Overfitting, in Proceedings of the 27th Symposium on the Interface of Computing Science and Statistics, pp. 352–360., 1995.

Schmid, H. P.: Footprint modeling for vegetation atmosphere exchange studies: a review and perspective, Agricultural and Forest Meteorology, 113(1–4), 159–183, doi:10.1016/S0168-1923(02)00107-7, 2002.

Skeeter, J.: June-Spaceboots/Illisarvik_CFluxes. [online] Available from: https://github.com/June-Spaceboots/Illisarvik_CFluxes (Accessed 3 December 2019), 2019.

Smith, M.: Neural Networks for Statistical Modeling, John Wiley & Sons, Inc., New York, NY, USA., 1993.

Sturtevant, C. S. and Oechel, W. C.: Spatial variation in landscape-level CO2 and CH4 fluxes from arctic coastal tundra: influence from vegetation, wetness, and the thaw lake cycle, Glob. Change Biol., 19(9), 2853–2866, doi:10.1111/gcb.12247, 2013.

Tetko, I. V., Livingstone, D. J. and Luik, A. I.: Neural network studies. 1. Comparison of overfitting and overtraining, Journal of Chemical Information and Modeling, 35(5), 826–833, doi:10.1021/ci00027a006, 1995.

Vickers, D. and Mahrt, L.: Quality Control and Flux Sampling Problems for Tower and Aircraft Data, http://dx.doi.org/10.1175/1520-0426(1997)014<0512:QCAFSP>2.0.CO;2 [online] Available from: http://journals.ametsoc.org/doi/abs/10.1175/1520-0426%281997%29014%3C0512%3AQCAFSP%3E2.0.CO%3B2 (Accessed 6 March 2017), 1997.

Vitale, D., Bilancia, M. and Papale, D.: A Multiple Imputation Strategy for Eddy Covariance Data, Journal of Environmental Informatics, 34(2), 68-87–87, 2018.

https://doi.org/10.5194/bg-2019-477
Preprint. Discussion started: 12 February 2020

Walter, K. M., Smith, L. C. and Chapin, F. S.: Methane Bubbling from Northern Lakes: Present and Future Contributions to the Global Methane Budget, Philosophical Transactions: Mathematical, Physical and Engineering Sciences, 365(1856), 1657–1676, 2007.

Webb, E., Pearman, G. and Leuning, R.: Correction of Flux Measurements for Density Effects Due to Heat and Water-Vapor Transfer, Q. J. R. Meteorol. Soc., 106(447), 85–100, doi:10.1002/qj.49710644707, 1980.

Weigend, A. S. and Lebaron, B.: Evaluating Neural Network Predictors by Bootstrapping, Humboldt University of Berlin, Interdisciplinary Research Project 373: Quantification and Simulation of Economic Processes. [online] Available from: https://ideas.repec.org/p/zbw/sfb373/199435.html (Accessed 21 January 2019), 1994.

Whalen, S. C. and Reeburgh, W. S.: Consumption of atmospheric methane by tundra soils, Nature, 346(6280), 160–162, doi:10.1038/346160a0, 1990.

Wilczak, J. M., Oncley, S. P. and Stage, S. A.: Sonic Anemometer Tilt Correction Algorithms, Boundary-Layer Meteorology, 99(1), 127–150, doi:10.1023/A:1018966204465, 2001.

Wilson, M. A., Burn C. R. and Humphreys E. R.: Vegetation Development and Variation in Near-Surface Ground Temperatures at Illisarvik, Western Arctic Coast, Cold Regions Engineering 2019, 687–695, doi:10.1061/9780784482599.079, 2019.

Zona, D., Oechel, W. C., Kochendorfer, J., Paw U, K. T., Salyuk, A. N., Olivas, P. C., Oberbauer, S. F. and Lipson, D. A.: Methane fluxes during the initiation of a large-scale water table manipulation experiment in the Alaskan Arctic tundra, Glob. Biogeochem. Cycle, 23, GB2013, doi:10.1029/2009GB003487, 2009.

Zona, D., Oechel, W. C., Peterson, K. M., Clements, R. J., U, K. T. P. and Ustin, S. L.: Characterization of the carbon fluxes of a vegetated drained lake basin chronosequence on the Alaskan Arctic Coastal Plain, Glob. Change Biol., 16(6), 1870–1882, doi:10.1111/j.1365-2486.2009.02107.x, 2010.

Zona, D., Lipson, D. A., Paw U, K. T., Oberbauer, S. F., Olivas, P., Gioli, B. and Oechel, W. C.: Increased CO2 loss from vegetated drained lake tundra ecosystems due to flooding, Glob. Biogeochem. Cycle, 26, GB2004, doi:10.1029/2011GB004037, 2012.

Zulueta, R. C., Oechel, W. C., Loescher, H. W., Lawrence, W. T. and Paw U, K. T.: Aircraft-derived regional scale CO2 fluxes from vegetated drained thaw-lake basins and interstitial tundra on the Arctic Coastal Plain of Alaska, Glob. Change Biol., 17(9), 2781–2802, doi:10.1111/j.1365-2486.2011.02433.x, 2011.

https://doi.org/10.5194/bg-2019-477
Preprint. Discussion started: 12 February 2020

615 **Figures & Tables**

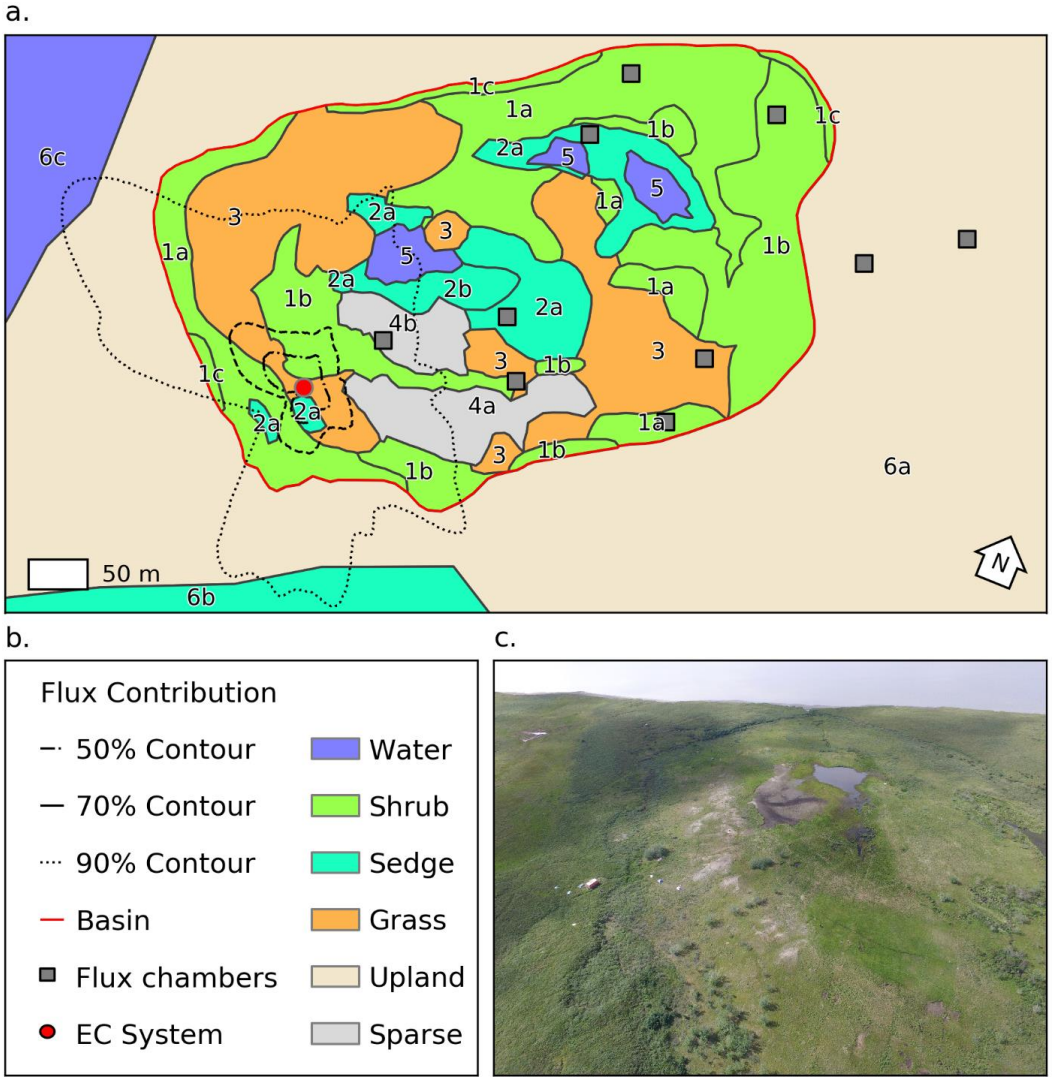

Figure 1: a) Map of the distribution of vegetation classes at Illisarvik, with the footprint climatology over the study period, the locations of the chambers and the eddy covariance (EC) system. The alphanumeric labels correspond to the unit codes in Table 1. b) Legend for the map in a. c) Oblique drone image of Illisarvik, take at 16:40 July 23rd 2016 view from E of
620 **DTLB towards W.**

https://doi.org/10.5194/bg-2019-477
Preprint. Discussion started: 12 February 2020

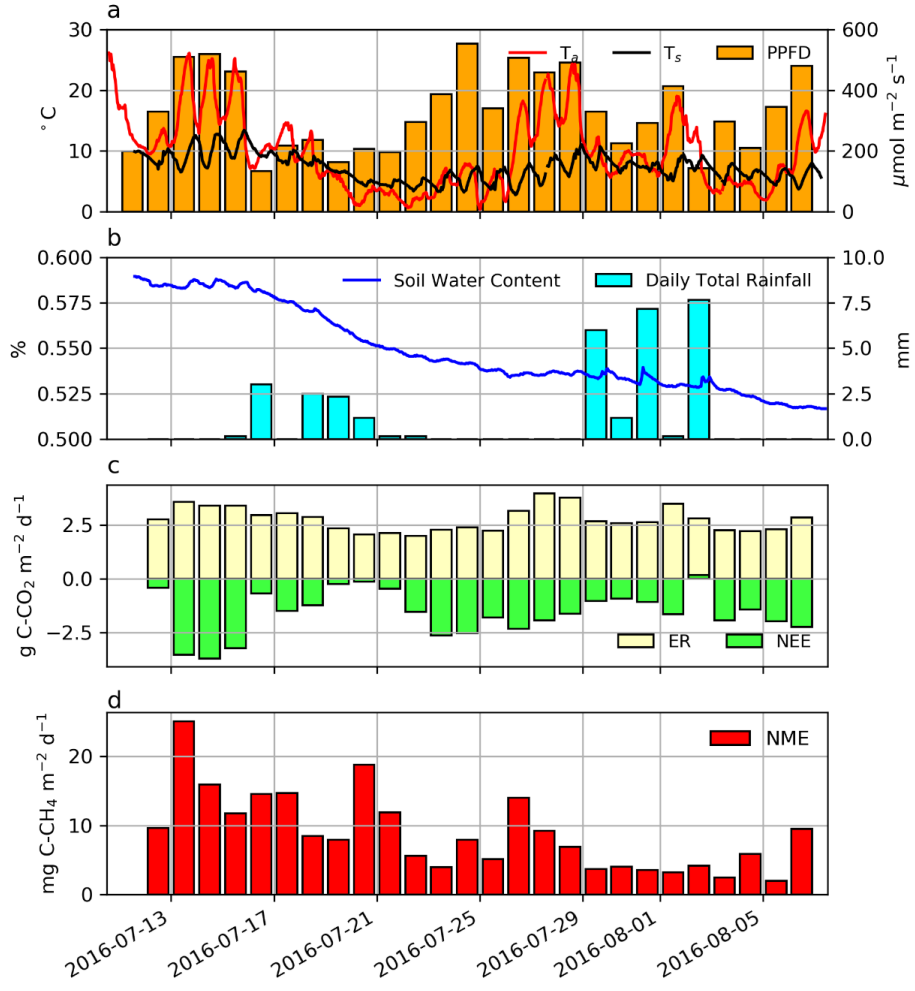

Figure 2: a) Half hourly air and soil temperatures, displayed along with photosynthetic photon flux density (PPFD). b) Hourly soil water content and daily total precipitation. c)Gap-filled daily total NEE (dark green), ER (red) and d) daily total NME.

https://doi.org/10.5194/bg-2019-477
Preprint. Discussion started: 12 February 2020

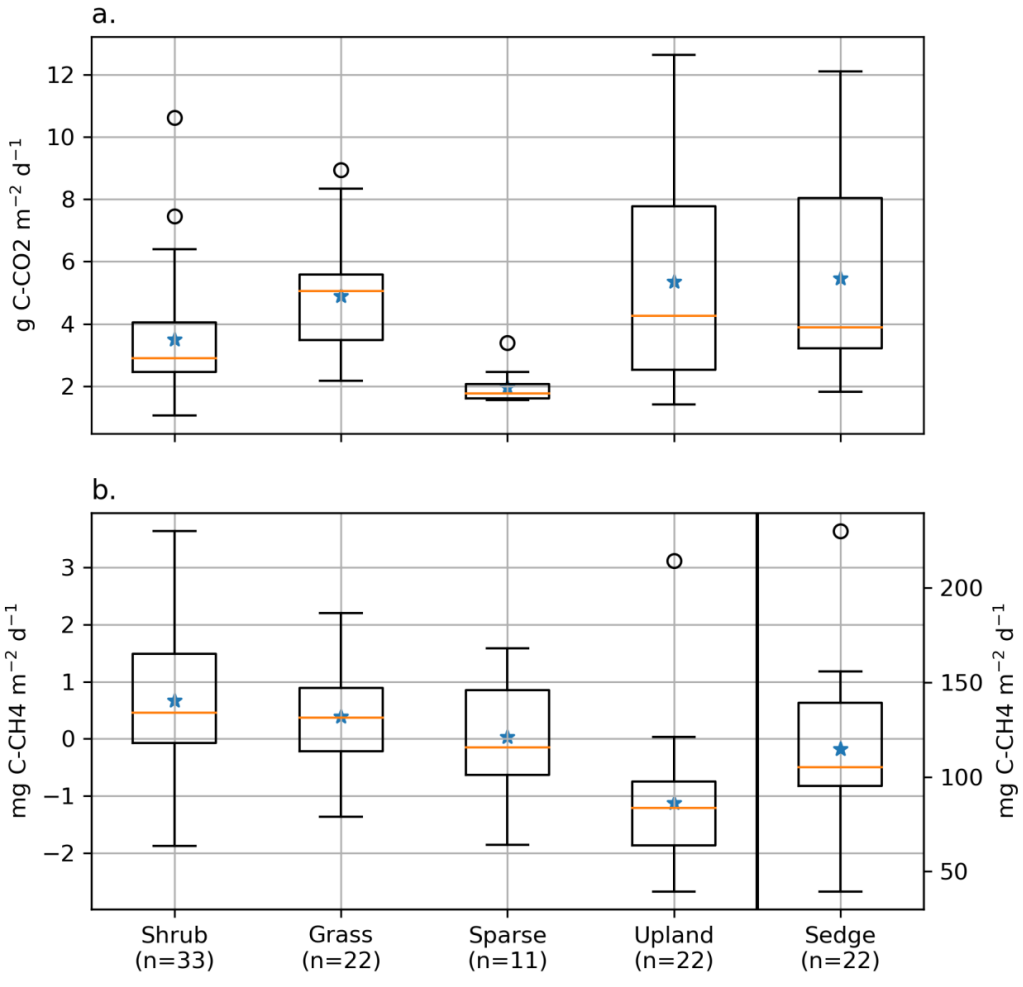

625

Figure 3: Boxplot of a) ER and b) NME fluxes measured using closed chambers, grouped by vegetation class. The orange lines represent the median, blue stars represent means, the boxes indicate the interquartile range (Q3-Q3), the whiskers indicate Q1 –(1.5*IQR) and Q3+(1.5*IQR), and the circles represent outliers extending beyond the whiskers. Note the scale for Sedge in b) is different.

https://doi.org/10.5194/bg-2019-477
Preprint. Discussion started: 12 February 2020

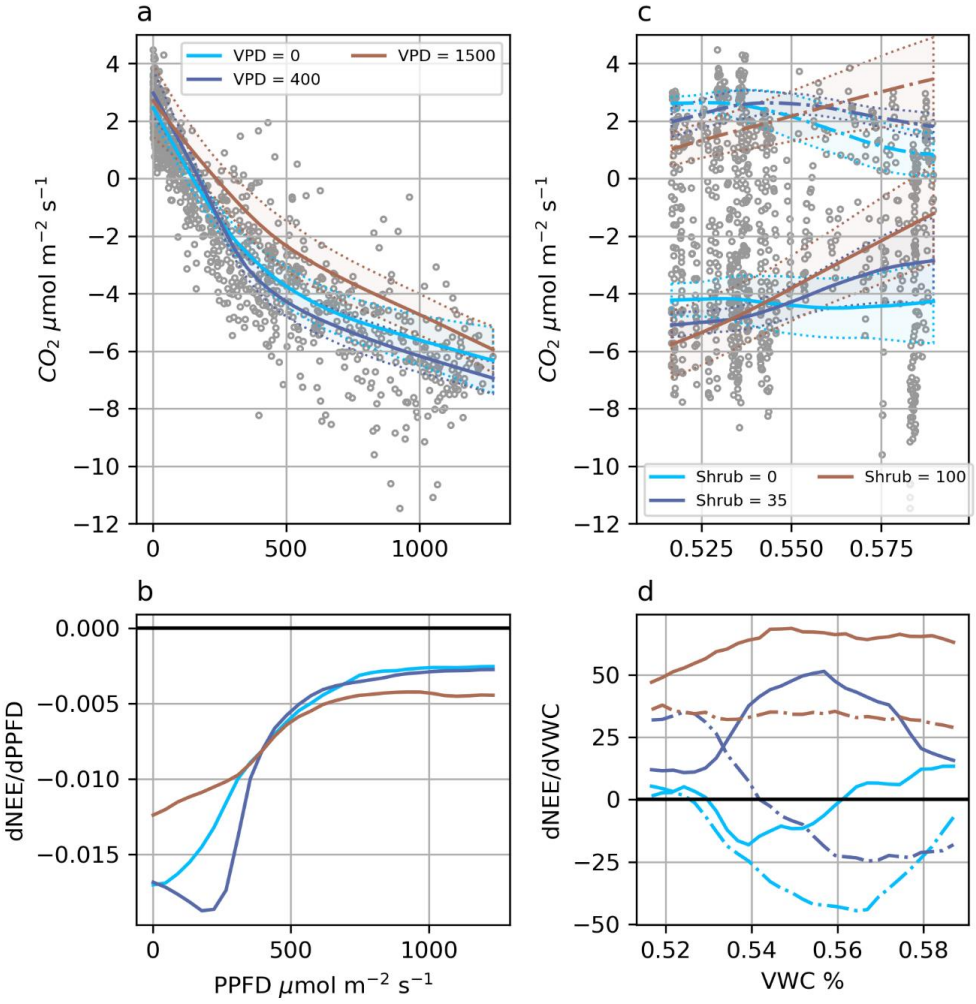

630

Figure 4: a. Modelled NEE response to PPFD under different VPD conditions and b. the partial first derivatives of NEE with respect to PPFD. c. Modelled ER (dashed line) and NEE (solid line) response to VWC at different Shrub$_{\%}$ and d. the partial first derivatives of ER (dashed lined) and NEE (solid line) with respect to VWC. NEE in c was calculated at PPFD = 600 umol m^2 s^{-1}. The shaded areas in a & c are 95% confidence intervals and grey circles are the EC observations.

https://doi.org/10.5194/bg-2019-477
Preprint. Discussion started: 12 February 2020

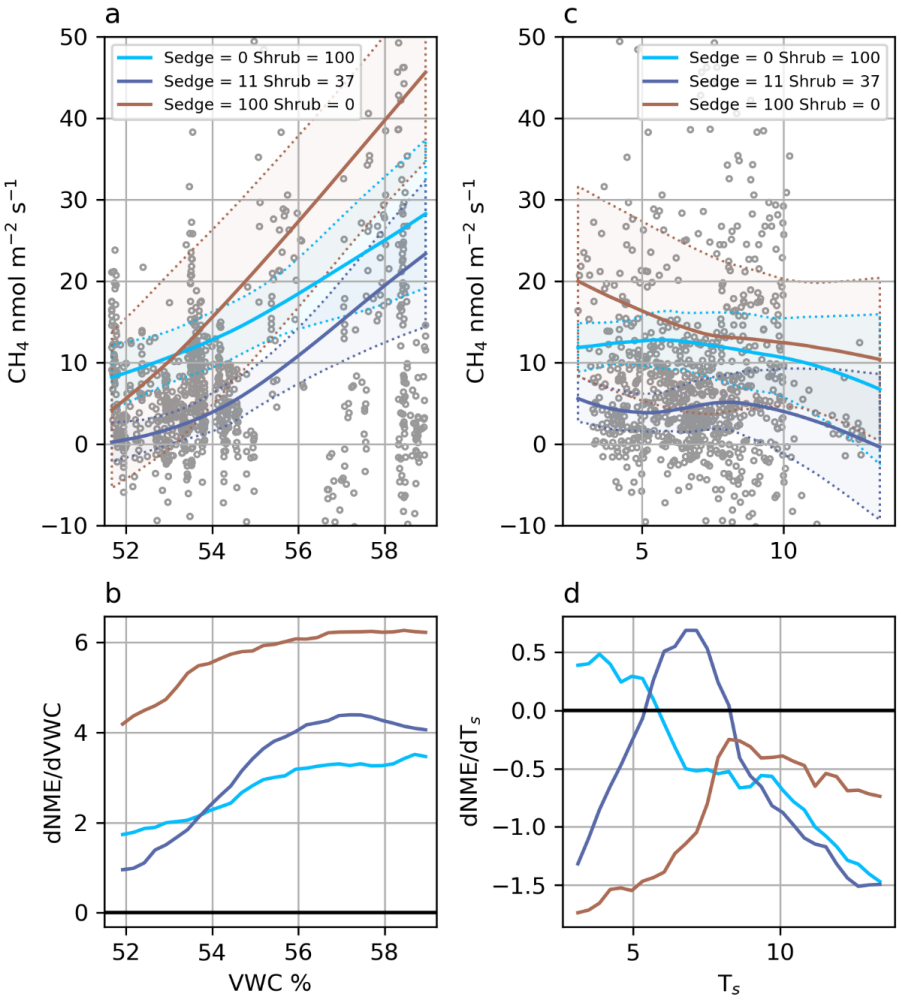

635

Figure 5: a. Modelled NME response to VWC at different source area fractions and b. the partial first derivatives of NME with respect to VWC. c. Modelled NME response to T_s at different source area fractions and d. the partial first derivatives of NME with respect to T_s. The shaded areas in a & c are 95% confidence intervals and grey circles are the EC observations.

https://doi.org/10.5194/bg-2019-477
Preprint. Discussion started: 12 February 2020

Biogeosciences
Discussions
Open Access
EGU

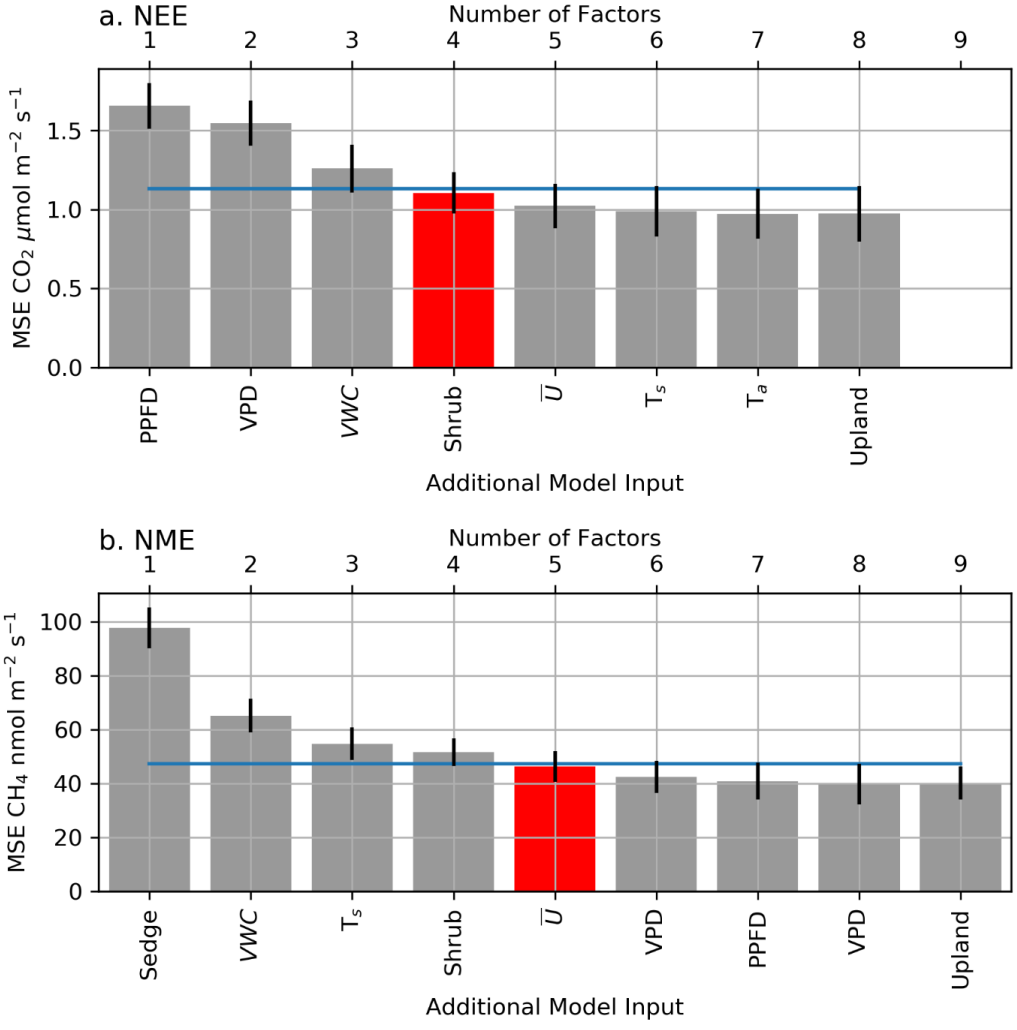

640

Figure A1: The averaged mean squared error (θ) of the bootstrapped validation datasets, with error bars showing one standard error (SE). The x axis shows models of increasing size from left to right (1-9 factors), and the label indicates the factor added to the model at each step. The blue line indicates the 1-SE rule threshold and the red bar indicates the model selected by the 1-SE rule.

645

https://doi.org/10.5194/bg-2019-477
Preprint. Discussion started: 12 February 2020

Biogeosciences Discussions Open Access EGU

Unit Code	Vegetation Class	Vegetation/Landscape feature
1a	Shrub	*Salix alaxnesis* (Tall Willow)
1b	Shrub	Salix spp. (Low Willows)
1c	Shrub	*Alnus* spp. (Alder)
2a	Sedge Marsh	*Carex* spp. (Sedge)
2b	Sedge Marsh	*Arctophila fulva* (Pendant Grass)
3	Grass Meadow	Pocacea spp. (Grass), *Eriophorum* (Cotton Grass)
4a	Sparse Cover	Sparse Vegetation
4b	Sparse Cover	Bare Ground
5	Ponds	*Hippuris* (Mare's Tail), Open Water
6a	Outside of Basin	Upland Tundra
6b	Outside of Basin	Fen
6c	Outside of Basin	Ocean

Table 1: Primary species and notable landscape feature present within the vegetation/cover classes. Unit codes correspond to the map Figure 1a.

Surface Class	Basin	Footprint
Shrub	48.3 %	36.0 % [0.0 – 79.0%]
Grass	27.9 %	39.0 % [1.1-78.1%]
Sedge	12.3 %	10.9 % [0.0 – 55.6%]
Sparse	8.4 %	2.2% [0.0 – 33.6%]
Water	3.1 %	0.2% [0.0 – 4.4%]
Upland	0%	6.2% [0.6 – 15%]
Outside Basin	0%	12.3% [0.2 - 28.0%]

Table 2: The surface cover class fractions of the basin, along with the mean source area fractions of the footprint climatology and the range of source area fractions for individual observations shown in brackets.

	Q_{10}	R_{10} μmol m^{-2} s^{-1}
Sedge	2.1	3.7
Upland	1.9	4.1
Grass	1.7	3.8
Shrub	1.7	2.7
Sparse	1.0	1.9
Night-time EC observations (n=100)	1.6	2.8

Table 3: The ER temperature sensitivity (Q_{10}) and base respiration (R_{10}) estimated by Laforce (2018) and estimated from nighttime footprint observations.